Journal Name

COMMUNICATION

Predicting the composition and formation of solid products in lithium-sulfur batteries by using an experimental phase diagram

Received 00th January 20xx,
Accepted 00th January 20xx

DOI: 10.1039/x0xx00000x

www.rsc.org/

J. W. Dibden, J. W. Smith, N. Zhou, N. Garcia-Araez* and J.R. Owen*

Lithium-sulfur batteries discharge via the transformation of solid sulfur to solid lithium sulfide via the formation of several polysulfide species that have only been observed in solution. Reported here is the first experimental phase diagram of a S_8-Li_2S-electrolyte system, which is shown to be a practical tool to determine the solution composition and formation of solid (S_8 and Li_2S) phases in lithium-sulfur batteries. The phase diagram is constructed by the combination of measurements of the total sulfur concentration $[S]_T$ and average oxidation state (S^{m-}) of polysulfide solutions prepared by reaction of S_8 and Li_2S. The phase diagram is used to predict the equilibrium discharge/charge profile of lithium-sulfur batteries as a function of the amount of electrolyte and the onset of precipitation and dissolution of solid products. High energy batteries should operate with a minimum amount of electrolyte, where both solid S_8 and Li_2S will be present during most of the charge and discharge of the cell, in which case we predict the observation of only one voltage plateau, instead of the two voltage plateaus commonly reported.

The lithium-sulfur rechargeable battery has been studied intensively as a candidate for the high specific energy market, which has applications in electric vehicles, portable devices and grid energy storage.[1-5] The theoretical specific energy is ca. 2600 W h kg^{-1}, which is notably higher than the lithium-ion battery. Several other advantages of using sulfur as the positive electrode include its abundance, low cost and non-toxicity. The theoretical specific capacity of sulfur (1672 A h kg^{-1}) is based on complete conversion from S_8 to Li_2S:

$$S_8 + 16\,Li^+ + 16\,e^- \rightarrow 8\,Li_2S \qquad \text{eq. 1}$$

The reduction of S_8 to Li_2S and reverse oxidation occur via multistep reaction pathways, which have led to the discharge and charge mechanisms being poorly understood compared with those of the lithium-ion battery.[6-9] Many previous studies have used spectroscopic methods to determine the nature of the several polysulfides that may be found in solution during discharge from S_8 to Li_2S and the reverse charge reaction.[7-12] By contrast, the contribution to the understanding of lithium-sulfur batteries that is made here is a purely thermodynamic treatment based on the equilibrium between three phases: solid S_8, solid Li_2S, and a solution of polysulfides in the electrolyte.[13, 14] For simplicity, we do not consider the existence of any other solids such as Li_2S_2, which is often suggested as a reaction intermediate, despite the fact that no crystal structure has been published. Only one publication suggested a ternary S_8-Li_2S-electrolyte phase diagram,[9] but it was not supported by experimental data. Here we report the first experimental phase diagram of the S_8-Li_2S-electrolyte system and apply it to explain the changes in electrolyte composition during the slow discharge and charge of lithium-sulfur batteries. We show that the phase diagram provides fundamental information about the thermodynamic equilibrium, which is a good approximation for slow cycling rates, and an essential starting point to study the kinetics at faster rates. Figure 1 illustrates the general form of the S_8-Li_2S-electrolyte phase diagram. The edges represent the binary mole fractions, x_i of each component, so that the bottom edge is related to the stoichiometry of Li_2S_n as follows:

$$\mathbf{x}_{\mathbf{Li_2S}} = \frac{[\mathbf{Li_2S}]}{[\mathbf{S}] + [\mathbf{Li_2S}]} = \frac{\mathbf{1}}{\boldsymbol{n}} \qquad \textbf{eq.2}$$

At the top of the diagram we find the one phase region where all the sulfur and Li_2S will dissolve forming a polysulfide solution. Next, we find two, two-phase regions representing the saturated solutions of each respective solid (sulfur + solution and Li_2S + solution, respectively); the curved upper boundaries show how the solubility of one solute increases with the concentration of the other. For example, starting from the saturated solution of sulfur in the pure solvent at point A, we follow a downward curve showing how adding lithium sulfide in solution increases the solubility of sulfur by reacting to form soluble polysulfides; similarly, point B signifies the solubility of lithium sulfide in pure solvent, and it increases with the addition of sulfur into the solution due to formation of different polysulfides. The two curves meet at point C, the

Chemistry, University of Southampton, SO17 1BJ, Southampton, United Kingdom.
E-mail: N.Garcia-Araez@soton.ac.uk and J.R.Owen@soton.ac.uk
Electronic Supplementary Information (ESI) available: See

congruent solution composition. This point represents the solution composition that is saturated with both components, i.e. in equilibrium with both solids (sulfur and Li_2S), and thus corresponds to the maximum concentration of all types of polysulfide species in a given electrolyte at a given temperature. This is also the composition of the solution throughout the 3-phase region (bottom) containing both solids.

Here we report a new experimental method to determine the first experimental ternary phase diagram of a S_8-Li_2S-electrolyte system. The method is used to characterize the reaction product of S_8 and Li_2S in a chosen electrolyte, providing the saturation composition as a function of the S_8/Li_2S ratio and the composition of the congruent solution where precipitation of solid products is expected. The electrolyte chosen for this study (1 M LiTFSI in 1,3-dioxolane) is used as a base model to represent the most commonly used electrolyte systems in lithium-sulfur batteries: 1 M LiTFSI in a mixture of 1,3-dioxolane with either dimethoxyethane or tetraglyme. But the methodology presented here will be easily applicable to other electrolyte systems where the solubilities of polysulfides can be dramatically different hence leading to fundamental changes in the reaction mechanism and kinetics.[15-17] The solvent dependence on the lithium-sulfur redox pathway has been suggested by Zou et al.,[17] who report that the type of electrolyte system affects the stability of the individual polysulfide species, making them more or less dominant.

Our method combines two types of experiments: determination of the total atomic sulfur concentration, $[S]_T^{sol.}$ by a gravimetric method and determination of the average oxidation state, S^{m-} (or average chain length, n in Li_2S_n), of polysufides by a redox titration. Some previous studies assumed that the solubility of polysulfide solutions of average chain length Li_2S_n could be determined by addition of excess of Li_2S and S_8 in a ratio of 1 to (n-1)/8 in a given solvent:

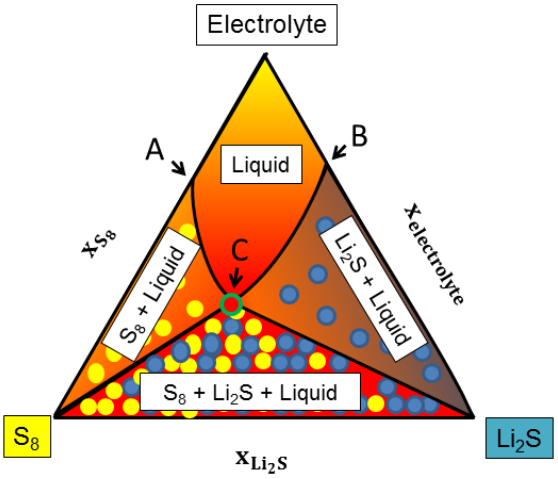

Fig. 1 Sketch of a ternary phase diagram of a S_8-Li_2S-electrolyte system.

$$Li_2S + \frac{n-1}{8} S_8 \rightarrow Li_2S_n \qquad \textbf{eq. 3}$$

In that approach, it was assumed that the average chain length of polysulfides dissolved in solution would depend on the relative amounts of Li_2S and S_8 added to the solution. It is shown here that this is not the case because the unreacted solid precipitate can be enriched in S_8 or Li_2S. Only in the one liquid region in the phase diagram (fig. 1) will Li_2S and S_8 fully dissolve upon reaction to form polysulfides, and only in the absence of solid precipitate will the average chain length of polysulfides (or average oxidation state) be given by the stoichiometry of Li_2S and S_8 added in solution.

Total atomic sulfur concentration of polysulfide solutions, $[S]_T^{sol.}$. There are few methods described in previous work to determine the saturation concentration of polysulfides, which here we report in terms of the total molar concentration of atomic sulfur. Park et al. used electrolysis to oxidize the polysulfide species to sulfur and the concentration was determined using UV-Vis spectroscopic measurements monitoring the absorbance at 266 nm, which correlated linearly to the concentration of sulfur.[18] Rauh et al. used methods suggested by Schwarzenbach and Fisher for the chemical analysis of polysulfides.[19, 20] This comprised of oxidizing the polysulfides to sulfate and performing a titration using barium perchlorate in the presence of a Thorin as an indicator, leading to precipitation as barium sulfate, $BaSO_4$. In this work, an approach similar to that undertaken by Schwarzenbach and Fisher was adopted. Gravimetric analysis was employed by oxidizing the polysulfide species to sulfate and precipitating as $BaSO_4$ (see supplementary information for details) The large relative molecular mass of $BaSO_4$ (233.43 g mol^{-1}) and low water solubility (ca. 2.5 µg mL^{-1}) make it ideal for gravimetric analysis improving the precision and accuracy of the results.[21]

Average oxidation state of sulfur in polysulfide solutions, S^{m-}. The speciation of lithium polysulfides has been intensely investigated in recent years. A variety of analytical techniques, often applied in operando, have been employed including X-ray adsorption and diffraction, Raman, UV-Vis, mass spectrometry, etc.[7, 8, 11, 12, 17, 22] This work uses a simple redox titration that is monitored by UV-Vis spectroscopy to determine the average oxidation state of the soluble polysulfide species. Rauh et al. used an iodometric redox titration[19] but we found that using the ferrocene/ferrocenium redox pair produced more accurate and reproducible results. Ferrocenium has a high enough potential to quantitatively oxidize polysulfides (+ 3.68 V vs. Li/Li^+) and changes from blue in its oxidized form to yellow in its reduced form.

$$2\,[Fe(C_5H_5)_2]^+\,(\text{blue}) + {S_n}^{2-} \rightarrow 2\,[Fe(C_5H_5)_2]\,(\text{yellow}) + \frac{n}{8} S_8 \qquad \textbf{eq. 4}$$

Ferrocenium possesses an absorption peak at 620 nm, a region where neither ferrocene nor S_8 absorb significantly, which makes it suitable for monitoring the progress of the reaction. The measurements will not be affected by the interference of the absorption by other polysulfide species, such as that of the S_3^- radical near 620 nm,[16, 17, 19] since ferrocenium is oxidizing

enough to quantitatively oxidize all polysulfides to sulfur, and hence ferrocenium and species such as S_3^- will not co-exist in equilibrium. Therefore, this redox titration method is a reliable approach to evaluate the average oxidation state of sulfur in the polysulfide solution. In order to facilitate the discussion of the results, the average chain length of polysulfides is calculated from the average oxidation state by considering that polysulfides are double-charged, Li_2S_n.

Construction of the phase diagram. To construct the phase diagram, mixtures of Li_2S and S_8 in an electrolyte (1 M LiTFSI in 1,3-dioxalane) were prepared at high concentration in order to identify the composition of the congruent solution, corresponding to the maximum solubility of all types of polysulfides. Such mixtures of solution + solids will be referred to as "blends". Blends of average composition of Li_2S_8 and Li_2S_6 were prepared, and the results of the analysis of the solution composition are summarized in table 1. The total atomic sulfur concentration in the blend, $[S]_T^{blend}$, was 10 M and 20 M, respectively. It is observed that a maximum atomic sulfur concentration of ca. 6 M in solution is achieved in blends of Li_2S_6 composition. Increasing the amount of solid starting material (from 10 M to 20 M in atomic sulfur) does not lead to a significant change in the solution composition, corroborating that the maximum polysulfide solubility has been reached. Blends of Li_2S_8 at 20 M concentration produce nearly the same solution composition, corroborating that this solution composition corresponds to the congruent point, beyond which it is not possible to dissolve more polysulfide. This example illustrates that the same solution composition, corresponding to the maximum solubility of polysulfides, will be reached provided that enough excess of both sulfur and Li_2S is included in the reaction mixture, and the composition will not depend on the ratio of Li_2S to S_8 employed. Finally, the analysis of the solution composition in the 10 M Li_2S_8 blend shows slightly smaller values of the total atomic sulfur concentration. This is because in this particular blend there is not enough Li_2S to form the congruent solution corresponding to 6 M of atomic sulfur concentration and average composition of Li_2S_4 (see details of calculations in the supplementary information). Therefore, the present results show that the composition of the congruent solution for this particular electrolyte, 1 M LiTFSI in 1,3-dioxolane, is ca. 6 M in atomic sulfur and has an average oxidation state of sulfur in polysulfides close to -0.5 (equivalent to Li_2S_4). The congruent solution is the solution composition in equilibrium with both S_8 and Li_2S, and hence this will be the actual solution composition of any practical Li-S battery designed for high energy, since dilution by the addition of an excess of electrolyte will have the detrimental effect of adding extra weight. The composition of the congruent solution for the electrolyte system under evaluation here is plotted in the experimental phase diagram in figure 2. Below this point, sulfur and Li_2S coexist in equilibrium with the congruent solution. The straight lines marking the separation between the 3-phase region and the two 2-phase regions are straight because the solution composition is constant. The lines marking the separation between the two 2-phase regions and the 1-phase region are drawn here tentatively taking into account the low solubility of sulfur and Li_2S. Further work is currently under development to determine the exact positions of the lines separating the one liquid region and the two liquid + solid regions.

Average composition in the blend	$[S]_T^{blend}$ / M	$[S]_T^{sol.}$ / M	Average oxidation state, S^{m-}	Average Li_2S_n chain length
Li_2S_8	10	4.1	0.40	5.0
Li_2S_8	20	5.3	0.41	4.9
Li_2S_6	10	5.9	0.41	4.8
Li_2S_6	20	6.3	0.48	4.2

Table 1 Analysis of highly concentrated polysulfide solutions using gravimetric analysis to determine the total atomic sulfur concentration of polysulfides in the solution, $[S]_T^{sol.}$, and UV-Vis redox titration to determine the average oxidation state of sulfur in polysulfide solutions, S^{m-}, and the average polysulfide chain length, i.e. *n* in Li_2S_n.

The phase diagram in figure 2 can now be used to rationalize the effect of the amount of electrolyte on the equilibrium discharge profile of Li-S cells. For simplicity, we will consider the formation of only one type of polysulfide with oxidation state of sulfur equal to $-m$, S^{m-}, but the same arguments could be expended to describe the formation of a variety of polysulfides. Line A in figure 2 illustrates a case where all the solid sulfur in the cell will be converted into soluble polysulfides, which then will be converted into Li_2S + solution. These two processes (sulfur conversion into polysulfides and polysulfide conversion into Li_2S) can be described by the Nernst equation and would lead to a discharge profile with two voltage plateaus (figure 3A):

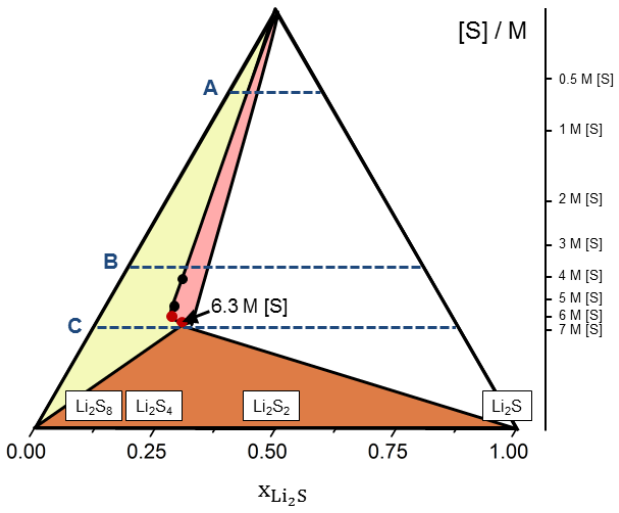

Fig. 2 Experimental ternary phase diagram of the system comprising of S_8, Li_2S and the electrolyte 1 M LiTFSI in 1,3-dioxolane. The diagram has been drawn using the results in table 1 for blends of average composition Li_2S_8 (black) and Li_2S_6 (red). Illustrations of three discharge trajectories of cells containing different initial amounts of electrolyte (A, B and C) are included.

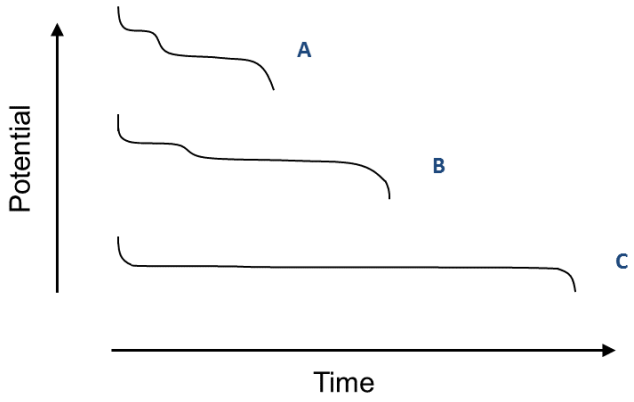

Fig. 3 Theoretical discharge profiles illustrating the change in plateau potential and capacity with sulfur content. For clarity, the discharge profiles have been shifted vertically.

$$E = E_1^0 + \frac{RT}{mF}\ln\frac{a_s}{a_{S^{m-}}} \qquad \text{eq.5}$$

$$E = E_2^0 + \frac{RT}{(2-m)F}\ln\frac{a_{S^{m-}}}{a_{S^{2-}}} \qquad \text{eq.6}$$

where a_S, $a_{S^{m-}}$ and $a_{S^{2-}}$ are the activities of S, S^{m-} and S^{2-} species (i.e. species with oxidation state of sulfur equal to zero, -*m* and -2, respectively), and E_1^0 and E_2^0 are the standard potentials of the S/S^{m-} and S^{m-}/S^{2-} couples, respectively. With a higher amount of initial sulfur in the cell (less electrolyte, line B in figure 2) the two plateaus will last longer and would be located closer together (figure 3B), since higher concentrations of polysulfides can be reached under these conditions, and this decreases the potential of the first plateau (eq. 5) and increases the potential of the second plateau (eq. 6). When the initial amount of the electrolyte in the lithium-sulfur cell is decreased further, eventually the saturation concentration of polysulfides will be reached (congruent solution, line C in figure 2), and the voltage of the cell will be constant and equal to:

$$E_3^0 = \frac{mE_1^0 + (2-m)E_2^0}{2} \qquad \text{eq. 7}$$

The corresponding equilibrium discharge profile is illustrated in figure 3C, and only one voltage plateau is expected according to the Nernst equation. With less electrolyte, in the region below curve C in fig. 2, the equilibrium discharge profile will show a true constant voltage plateau in the 3-phase region merged together with the nearly constant voltage plateaus predicted by the Nernst equation. There is experimental evidence supporting the formation of only one plateau in the equilibrium discharge profile (evaluated by GITT experiments from the values of the rest potential) under conditions where the maximum solubility of polysulfides is reached in the Li-S cell.[23] This work was done in a new class of electrolyte with minimal solubility for polysulfides. Achieving the maximum polysulfide concentration in cells with 1,3-dioxolane as the solvent is much more challenging due to the much higher polysulfide solubility (ca. 6 M in 1 M LiTFSI), which leads to problems of interference of polysulfide shuttling to the lithium electrode. Polysulfide shuttling is not taken into account in the prediction of discharge profiles made here, but it will lead to a significant decrease in the measured discharge capacity.

In conclusion, this work reports an accurate and reliable method to determine the ternary phase diagram of sulfur-Li_2S-electrolyte system and its application in predicting the phase composition and equilibrium (dis)charge profile of Li-S cells.

James W. Dibden acknowledges Oxis Energy Ltd., the University of Southampton and EPSRC (EP/M50662X/1) for a CASE studentship.

Notes and references

1. X. Ji, K. T. Lee and L. F. Nazar, *Nat Mater*, 2009, **8**, 500-506.
2. X. L. Ji and L. F. Nazar, *J. Mater. Chem.*, 2010, **20**, 9821-9826.
3. A. Manthiram, S.-H. Chung and C. Zu, *Adv. Mater.*, 2015, **27**, 1980-2006.
4. P. G. Bruce, S. A. Freunberger, L. J. Hardwick and J. M. Tarascon, *Nat. Mater.*, 2012, **11**, 19-29.
5. S. Thieme, J. Bruckner, A. Meier, I. Bauer, K. Gruber, J. Kaspar, A. Helmer, H. Althues, M. Schmuck and S. Kaskel, *J. Mater. Chem. A*, 2015, **3**, 3808-3820.
6. S. Evers and L. F. Nazar, *Acc. Chem. Res.*, 2013, **46**, 1135-1143.
7. H.-L. Wu, L. A. Huff and A. A. Gewirth, *ACS Appl. Mater. Inter.*, 2014, **7**, 1709-1719.
8. S. Walus, C. Barchasz, J. F. Colin, J. F. Martin, E. Elkaim, J. C. Lepretre and F. Alloin, *Chem. Commun.*, 2013, **49**, 7899-7901.
9. K. A. See, M. Leskes, J. M. Griffin, S. Britto, P. D. Matthews, A. Emly, A. Van der Ven, D. S. Wright, A. J. Morris, C. P. Grey and R. Seshadri, *J. Am. Chem. Soc.*, 2014, **136**, 16368-16377.
10. Q. Wang, J. M. Zheng, E. Walter, H. L. Pan, D. P. Lv, P. J. Zuo, H. H. Chen, Z. D. Deng, B. Y. Liaw, X. Q. Yu, X. Q. Yang, J. G. Zhang, J. Liu and J. Xiao, *J. Electrochem. Soc.*, 2015, **162**, A474-A478.
11. M. U. M. Patel, R. Demir-Cakan, M. Morcrette, J. M. Tarascon, M. Gaberscek and R. Dominko, *ChemSusChem*, 2013, **6**, 1177-1181.
12. M. Cuisinier, P. E. Cabelguen, S. Evers, G. He, M. Kolbeck, A. Garsuch, T. Bolin, M. Balasubramanian and L. F. Nazar, *J. Phys. Chem. Lett.*, 2013, **4**, 3227-3232.
13. J. R. Owen, presented in part at LiSM[3], London, 2016.
14. J. W. Dibden, poster (# P1-0764) presented at the 18th International Meeting on Lithium Batteries, Chicago, 2016.
15. M. Wild, L. O'Neill, T. Zhang, R. Purkayastha, G. Minton, M. Marinescu and G. J. Offer, *Energ. Environ. Sci.*, 2015, **8**, 3477-3494.
16. Y.-C. Lu, Q. He and H. A. Gasteiger, *J. Phys. Chem. C*, 2014, **118**, 5733-5741.
17. Q. Zou and Y.-C. Lu, *J. Phys. Chem. Lett.*, 2016, **7**, 1518-1525.
18. J. W. Park, K. Yamauchi, E. Takashima, N. Tachikawa, K. Ueno, K. Dokko and M. Watanabe, *J. Phys. Chem. C*, 2013, **117**, 4431-4440.
19. R. D. Rauh, F. S. Shuker, J. M. Marston and S. B. Brummer, *J. Inorg. Nucl. Chem.*, 1977, **39**, 1761-1766.
20. G. Schwarzenbach and A. Fischer, *Helv. Chim. Acta*, 1960, **43**, 1365-1390.
21. D. R. Lide, *CRC Handbook of Chemistry and Physics, 85th Edition*, Taylor & Francis, 2004.
22. J. Gun, A. D. Modestov, A. Kamyshny, Jr., D. Ryzkov, V. Gitis, A. Goifman, O. Lev, V. Hultsch, T. Grischek and E. Worch, *Microchim. Acta*, 2004, **146**, 229-237.
23. M. Cuisinier, P. E. Cabelguen, B. D. Adams, A. Garsuch, M. Balasubramanian and L. F. Nazar, *Energ. Environ. Sci.*, 2014, **7**, 2697-2705.

